MNRAS **000**, 1–5 (2018) Preprint 1 November 2018 Compiled using MNRAS LaTeX style file v3.0

Super-Earths in the TW Hya disc

Daniel Mentiplay[1]*, Daniel J. Price[1] and Christophe Pinte[1,2]
[1] *Monash Centre for Astrophysics (MoCA) and School of Physics and Astronomy, Monash University, Clayton Vic 3800, Australia*
[2] *Univ. Grenoble Alpes, CNRS, IPAG, F-38000 Grenoble, France*

ABSTRACT

We test the hypothesis that the dust and scattered light gaps seen in recent observations of TW Hya are caused by planet-disc interactions. We perform global three-dimensional dusty smoothed particle hydrodynamics simulations, comparing synthetic observations of our models with dust thermal emission, CO emission and scattered light observations. We find that the dust gaps observed at 24 au and 41 au can be explained by super-Earth to super-Neptune mass planets ($\sim$ 8–24 $\mathrm{M}_{\oplus}$). A planet of Saturn-mass or higher can explain the depth and width of the gap seen in scattered light at 94 au. Our model produces a prominent spiral arm while there are only hints of this in the data. To avoid runaway growth and migration of the planets, and to produce axisymmetric rings in mm dust emission, we require a disc mass of $\lesssim 10^{-3}\,\mathrm{M}_{\odot}$ in agreement with CO observations but 10–100 times lower than the estimation from HD line emission.

Key words: protoplanetary discs — planet-disc interactions — hydrodynamics — stars: individual (TW Hydrae) — submillimetre: planetary systems — infrared: planetary systems

1 INTRODUCTION

TW Hya, our nearest gas-rich protoplanetary disc, was recently imaged by ALMA at 870 μm (Andrews et al. 2016). These observations of thermal emission from $\sim$100μm dust in the midplane show a series of stunning axisymmetric gaps. At just 60 pc (Gaia Collaboration et al. 2018) TW Hya presents a unique opportunity to observe planet formation on our doorstep. Being a member of the 3–20 Myr old (Barrado Y Navascués 2006) TW Hya association means TW Hya is older than the typical disc lifetime of $\sim$ 3 Myr (Haisch et al. 2001) implying that planet formation should almost be complete.

van Boekel et al. (2017) observed TW Hya in polarized scattered light using the Spectro-Polarimetric High-contrast Exoplanet REsearch (SPHERE) instrument on the Very Large Telescope. Scattered light observations trace the small grains in the upper layers of the gas disc. These grains are tightly coupled to the gas via drag. Of the two main gaps in the sub-mm dust emission (at 24 au and 41 au) only the inner gap is observed in the scattered light image.

Estimates of the gas mass in TW Hya vary over several orders of magnitude. Thi et al. (2010) use radiative transfer modelling of CO emission to infer a gas mass $(0.5–5) \times 10^{-3}\,\mathrm{M}_{\odot}$. Whereas Bergin et al. (2013) use hydrogen deuteride (HD) observations to infer a disc mass $> 0.05\,\mathrm{M}_{\odot}$. At this mass the self-gravity of the disc is significant and gravitational instability may lead to disc fragmentation (Kratter & Lodato 2016).

The characteristic timescale for aerodynamic drag to act on dust grains is determined by the dimensionless stopping time, or Stokes number, St (Weidenschilling 1977; Takeuchi & Lin 2002). The Stokes number controls the rate of vertical settling and radial drift. The Stokes number is proportional to the grain size and inversely proportional to the gas density. Small grains ($\sim$ μm) experience high drag and have low St. Whereas large grains ($\gtrsim$ cm) are largely decoupled from the gas phase and have high St. Grains with St $\sim$ 1 experience the greatest rate of settling and drift and lead to the formation of axisymmetric rings (Ayliffe et al. 2012; Dipierro et al. 2015). The different response of small and large grains to gas drag can be used to infer the mechanism for the origin of the gaps.

To reproduce the axisymmetric gaps observed in recent ALMA observations, various mechanisms have been proposed, including: planet-disc interactions (Dipierro et al. 2015), self-induced dust trapping (Gonzalez et al. 2017), vortices (Zhu & Stone 2014), condensation fronts (Zhang et al. 2015), non-ideal MHD effects (Béthune et al. 2016) and zonal flows (Johansen et al. 2009; Flock et al. 2015).

In this Letter, we explore the hypothesis that the axisymmetric rings and gaps in the TW Hya disc are carved by planets. Our approach is similar to Dipierro et al. (2015) who explored a similar hypothesis for HL Tau. We aim to constrain the planet masses required to explain the observational data on TW Hya and to motivate follow up observations.

* daniel.mentiplay@monash.edu

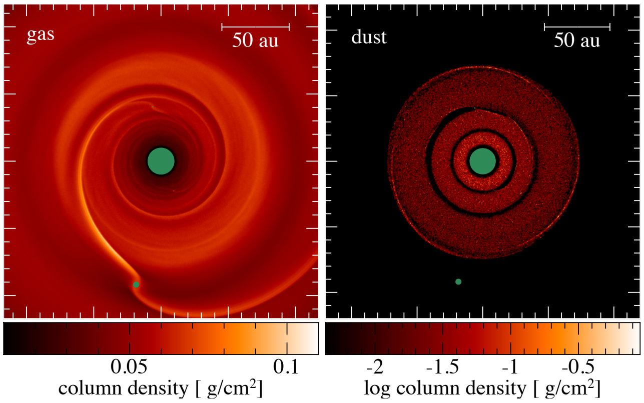

Figure 1. Gas (*left*) and dust (*right*) surface density for the model with 8 $\mathrm{M}_\oplus$ inner planets (24 and 41 au) and 0.3 $\mathrm{M_J}$ outer planet (94 au) after 14660 years. The green markers are sink particles with radius proportional to accretion radius. We do not model the inner ($\lesssim$ 10 au) disc. The outer edge of the dust disc is $\sim$ 70 au.

2 METHODS

2.1 Numerical method

We perform 3D global simulations of a dusty gas disc with embedded protoplanets using PHANTOM, a smoothed particle hydrodynamics (SPH) code (Price et al. 2017). Dust interacts with the gas via a drag force. This allows the dust to settle to the midplane and to migrate radially. The dust also interacts gravitationally with the central star and embedded planets. We use a low disc mass, so the disc is not self-gravitating.

We simulate only one dust grain size. We choose 100 μm grains with St $\sim$ 1 to ensure efficient settling and radial migration of our simulated grains. In this regime it is appropriate to use the two-fluid method (Laibe & Price 2012). We use 10^7 particles for the gas, and 2.5×10^5 for the dust. We use a greater number of gas particles to prevent dust becoming trapped under the gas resolution scale (Laibe & Price 2012). For 100 μm-sized grains, the gas mean free path is large compared with the grain size, and so we assume Epstein drag Epstein (1924). We assume spherical grains with a material density of 3 g cm^{-3}. We also perform gas-only simulations to explore the impact of the outer planet.

We use sink particles (Bate et al. 1995) to represent the central star and three embedded protoplanets. The sink particles interact gravitationally with the disc and with each other. Gravitationally bound dust and gas within the accretion radius is accreted onto the sink. For computational efficiency, we set the stellar accretion radius to be the inner edge of the disc.

2.2 Initial conditions

We assume a distance of 59.5 au (Gaia Collaboration et al. 2016) and a stellar mass of 0.8 $\mathrm{M}_\odot$ (Andrews et al. 2012). Scattered light and CO line observations show that the gas disc extends out to at least $\sim$200 au (Thi et al. 2010) so we take the outer edge of the gas disc to be 200 au. We set the inner edge of the disc to be $R_{\rm in}$ = 10 au for computational efficiency. We do not attempt to model the inner disc ($\lesssim$ 10 au) in this study.

We set up a disc consisting of SPH particles following Lodato & Price (2010). We assume a gas mass of $7.5 \times 10^{-4}\,\mathrm{M}_\odot$ (within the annulus from 10 au to 200 au) which is in the low end of the Thi et al. (2010) range. We set the initial surface density profile as a smoothed power law: $\Sigma = \Sigma_{\rm in}(R/R_{\rm in})^{-p}(1-\sqrt{R_{\rm in}/R})$, where we adopt a shallow surface density profile with $p = 0.5$. This, with our gas disc mass, gives a surface density of $\Sigma \approx 0.05-0.08$ g cm^{-2}, corresponding to a Stokes number of St $\approx 0.25-0.4$ for 100 μm grains.

We assume a vertically isothermal equation of state $P = [c_s(R)]^2\rho$ with $T = 30\,\mathrm{K}(R/R_{\rm in})^{-0.25}$ where $c_s^2 = k_B T/\mu m_p$. This is determined by matching the CO snowline (20 K at 19 au) from van't Hoff et al. (2017) together with a midplane temperature of 15 K at 60 au following previous modelling (Andrews et al. 2012). From these we infer a disc aspect ratio of $H/R = c_s/(\Omega R) = 0.034$ at $R_{\rm in}$. Flaherty et al. (2018) provide an upper limit on the turbulent velocity in the outer disc of $v_{\rm turb}/c_s \approx 0.04-0.13$. This corresponds to an $\alpha \sim (v_{\rm turb}/c_s)^2 \lesssim 0.002 - 0.02$. We choose a disc viscosity (Shakura & Sunyaev 1973) at the lower end of this range and set the SPH artificial viscosity to $\alpha_{\rm AV} = 0.1$ giving $\alpha \sim 0.001$.

The dust disc is much more compact than the gas disc. Thermal emission from the dust shows that the sub-mm dust disc extends to $\sim$ 50 au (Andrews et al. 2016). We set the outer edge of the dust disc to $R_{\rm out}$ = 80 au, just inside the orbital radius of the outer planet. This is to allow for some radial drift, without having to follow the drift of dust particles from the gas outer radius. We use the same inner edge as for the gas disc. Dust disc mass estimates are in the range (2–6) $\times 10^{-4}\,\mathrm{M}_\odot$ (Calvet et al. 2002; Thi et al. 2010). With our gas disc mass this gives a dust-to-gas ratio of $\approx$ 0.25–0.8 which is one to two orders of magnitude higher than the typical interstellar value. However, TW Hya is an old disc within which we can expect significant evolution away from its initial conditions. We set the dust-to-gas ratio (for 100 μm grains) to 0.05.

2.3 Embedded planets

We assume two super-Earth to super-Neptune mass planets at 24 au and 41 au, respectively, to reproduce the two main observed gaps in sub-mm emission (Andrews et al. 2016). We explored masses in the range of 4–24 $\mathrm{M}_\oplus$ for these planets. To reproduce the outer gap observed in scattered light (van Boekel et al. 2017) we placed a more massive planet at 94 au. We explored a range of masses for the outer planet between 0.1–2 $\mathrm{M_J}$. We set the planetary accretion radius $R_{\rm acc}$ to half the Hill radius, $R_{\rm H} = a\sqrt[3]{m_{\rm p}/3M_*}$, where a is the semi-major axis, and $m_{\rm p}$ and M_* are the planet mass and stellar mass, respectively. Accretion proceeds unchecked for particles within 80% of the accretion radius.

2.4 Synthetic observations

We use the 3D radiative transfer code MCFOST (Pinte et al. 2006, 2009) to post-process the PHANTOM output to produce simulated ALMA band 7 images, CO maps and polarized scattered light images. We use a Voronoi (unstructured) mesh using Voro++ (Rycroft 2009) in which the computational domain is subdivided into cells generated from the positions of the SPH gas particles. We assume an inclination of 5° and position angle 152° (Huang et al. 2018) when making synthetic observations of the disc.

Within each cell we split the distribution of dust grain sizes into 100 logarithmic bins from 0.03 μm to 1 mm. Grains smaller than 1 μm are assumed to trace the gas. Grains larger than 100 μm are assumed to trace the dust particles. Grains of intermediate size are interpolated between the gas and dust. The total dust mass is

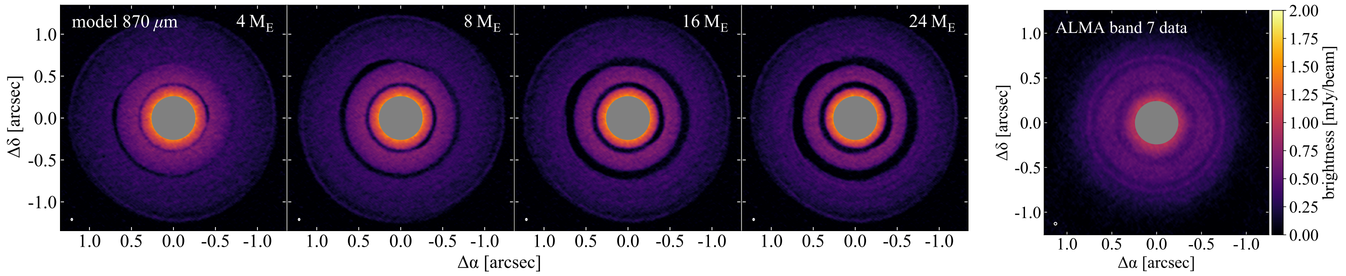

Figure 2. Inner planets (24 and 41 au). Synthetic observations of dust thermal emission at 870 μm, compared with ALMA band 7 observations from Andrews et al. (2016). From left to right: dust+gas models with 4, 8, 16, 24 $M_\oplus$ inner planets. The beam has FWHM 28×21 mas in the model image, compared with 30 mas FWHM (1.6 au) circular beam in the observations. We obscured the inner ≈15 au as we did not model that region.

set to $2.5 \times 10^{-4}\,M_\odot$. We use 10^7 photon packets to determine the temperature structure and 10^7 photon packets per wavelength to produce synthetic observations.

We use the Common Astronomy Software Application (CASA) ALMA simulator (version 4.7) to produce synthetic band 7 ALMA images at 870 μm to compare with Andrews et al. (2016). We use a transit duration of 45 minutes, add thermal noise from the receivers and atmosphere, and set the precipitable water vapour to 0.5 mm. To match the beam size of the observations, we choose an ALMA antenna configuration (cycle 3.8) which gives a beam of FWHM 28×21 mas at PA $= -60.3°$.

We post-process gas-only PHANTOM simulations in MCFOST to produce polarized scattered light images, and CO emission maps, assuming the dust follows the gas. In these calculations we assume a dust-to-gas ratio of 0.01. From 1.6 μm (H-band) scattered light maps we calculated the azimuthal Stokes component Q_ϕ, scaled by R^2. We then we add Gaussian noise and convolve with a Gaussian beam with a FWHM of 48.5 mas, following the H-band SPHERE observations in van Boekel et al. (2017).

We also produce CO emission maps in the J = 3 — 2 line. We assume $T_{\rm gas} = T_{\rm dust}$ and that the emission is at LTE, as we are looking at low-J CO lines. We assume a CO-to-H_2 molecular abundance of 10^{-4}. We produce channel maps at 0.1 km/s resolution to then calculate the M_0 moment map. We convolve with a Gaussian beam with FWHM of 139×131 mas with a PA $= -74.9°$ following the ALMA observations presented by Huang et al. (2018).

3 RESULTS

Figure 1 shows the gas and dust surface density after 14660 years (125, 50, and 16 orbits of the 24, 41, and 94 au planets, resp.) for the model with 8 $M_\oplus$ inner planets (24 and 41 au) and 0.3 M_J outer planet (94 au). The dust disc extends to $\sim$ 70 au (*right* of Figure 1). We note that there was negligible planetary migration. We observe cleared dust gaps at the locations of the two inner planets, while the planets are not massive enough to carve gaps in the gas (Figure 1). The Saturn-to-Jupiter-mass outer planet carves a (partial) gap in the gas, and produces a spiral density wave. The region interior to 10 au is devoid of dust merely because it is within the accretion radius of the stellar sink particle.

3.1 Dust thermal emission

Figure 2 compares our synthetic band 7 ALMA observations of dust thermal continuum emission for models with 4, 8, 16, and 24 $M_\oplus$ inner planets with the ALMA observations (Andrews et al. 2016). Low mass planets ($< 0.1\,M_J \approx 32\,M_\oplus$) successfully reproduce the width and axisymmetry of the observed gaps at 24 and 41 au.

Increasing the planet mass increases the gap width, as expected. No gap is opened by a 4 $M_\oplus$ planet at 41 au. The lowest mass planets that can produce almost axisymmetric gaps for our disc model at both 24 and 41 au is $\approx 8\,M_\oplus$. The planet mass with gap width closest in size to the ALMA gap width of ≈ 5 au depends on orbital radius. Our results suggest that to carve a 5 au gap at 24 au in the 100 μm dust disc requires a planet mass of 16–24 $M_\oplus$. Similarly, to carve a 5 au gap at 41 au in the 100 μm dust disc requires a planet mass of 8–16 $M_\oplus$. This suggests that the 24 au planet is more massive than the 41 au. This finding is consistent with the scattered light observations, which show a low contrast gap at 24 au but none at 41 au. A planet mass of 16–24 $M_\oplus$ for the innermost planet is also consistent with an upper limit suggested by Nomura et al. (2016). It is also consistent with modelling from van Boekel et al. (2017) following Duffell & Dong (2015), and with the low-viscosity models of Dong & Fung (2017).

3.2 Scattered light and CO emission

Figure 3 (*top*) compares our synthetic polarized scattered light H-band observations for gas-only models with outer planet masses 0.1, 0.3, 1, and 2 M_J, with the SPHERE observation from van Boekel et al. (2017). The spiral density wave induced by the outer planet is visible in all of our synthetic observations. For the 0.3, 1, and 2 M_J we observe a dip in scattered light at the orbital radius of the planet. Figure 4 quantifies this by comparing the azimuthally-averaged brightness profile for each model. The brightness contrast between the peak and gap for a Saturn to Jupiter mass (0.3–1 M_J) planet is consistent with the SPHERE observation. A 0.1 M_J planet, by contrast, fails to reproduce the gap.

Figure 3 (*bottom*) compares synthetic CO J = 3 — 2 emission maps for gas-only models with outer planet masses 0.1, 0.3, 1, and 2 M_J, with the ALMA observations (Huang et al. 2018). The 0.3–1 M_J models, which best fit the scattered light radial profile, is consistent with CO observations. For a planet larger than 0.3 M_J, the gas surrounding the planet is visible in the M_0 map. This is because we have infinite signal-to-noise in our model. The gas surrounding the planet has a perturbed velocity field and is emitting in a large number of channels. While the signal in each channel is faint and would not have been detected by ALMA, when aggregated in the M_0 map, it becomes visible. Higher S/N ALMA observations might be able to detect such a signal.

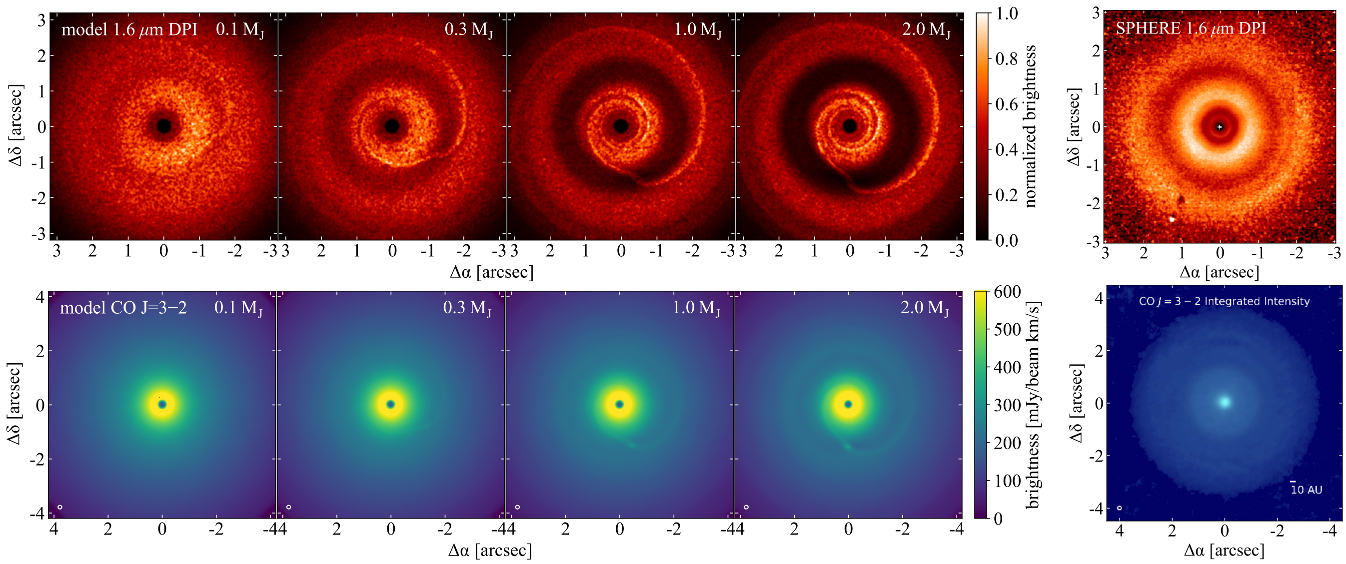

Figure 3. Gas-only models with outer planet (94 au) masses 0.1, 0.3, 1, and 2 M_J after 45 orbits. *Top*: Comparison of synthetic observations of 1.6 μm polarized intensity scaled by R^2 with the SPHERE observation. We convolved with a circular Gaussian beam of FWHM 48.5 mas, and added Gaussian noise. *Bottom*: Comparison of synthetic CO J = 3 — 2 integrated intensity emission maps with the ALMA observation. We convolved with a Gaussian beam of 139×131 mas with a PA $= -74.9°$. The top and bottom right panels are reproduced from van Boekel et al. (2017) and Huang et al. (2018), respectively.

4 DISCUSSION

For computational efficiency we did not model the inner disc (within $\sim$ 10 au). This leads to a hotter temperature at radii $\lesssim$ 15 au, where the stellar radiation directly hits the dust. Thus the dust thermal emission within the innermost planet orbit is larger than the observation. We checked that the temperature at the location of the planet is not affected by this, and the corresponding fluxes are correct.

The overall flux is consistent to within a factor of 2 of the ALMA observation. However, the contrast in flux between our gaps and rings is greater than the observed contrast. The emission gaps are only 5–20% fainter than the rings in the ALMA observations (Andrews et al. 2016). Whereas the model gaps are 60–80%. This is likely due to our choice to only simulate one grain size for the population of large grains. We expect there to be additional flux contributed from nearby grain sizes that we have not included in our calculation. These grains will have a different Stokes number than the 100-μm-grains and will be less effected by the dynamical gap opening of the planets, thus filling out the flux in the gap. Multigrain dust simulations that include a range of grain sizes that contribute to the emission wavelength may alleviate that problem (Hutchison et al. 2018).

Spectral index observations from Huang et al. (2018) suggest that within the gaps the maximum grain size is at most a few mm, whereas in the bright rings cm grains are present. In this case, the gas disc mass may be an order of magnitude higher, such that the mm grains have similar Stokes number to the 100 μm grains in our calculations.

There is a tension between the outer planet mass required to reproduce the gap in scattered light and CO observations, and the mass required to hide a spiral density wave. The synthetic observation from the 0.3 M_J model (top of Figure 3) shows a greater degree of azimuthal asymmetry than the SPHERE observation. Models with a lower mass planet ($\sim 0.1\,M_J$) are more azimuthally symmetric. However, at those masses we fail to reproduce the gap in both scattered light and in CO emission. A mass of 0.3 $M_J \approx 95\ M_\oplus$ is higher than suggested by previous authors (Dong & Fung 2017; van Boekel et al. 2017). It is possible that we are overestimating the planet mass if the gap were accentuated by shadowing from the inner disc (Debes et al. 2013, 2017; Poteet et al. 2018).

For our disc model, the stellar accretion rate is $1.5 \times 10^{-10}\,M_\odot\,yr^{-1}$ which is an order of magnitude below the estimated rate (Brickhouse et al. 2012). The accretion rate is given by $\dot{M} = 3\pi\Sigma\alpha c_s H$. This suggest two modifications to our model to increase $\dot{M}$: we could increase the disc mass, and we could increase the disc viscosity. The are problems with both approaches. Increasing the disc mass changes the Stokes number of grains. The viscosity is constrained by observations (Flaherty et al. 2018). An alternative may be that accretion is driven by winds (Simon et al. 2017) rather than a disc viscosity.

Increasing the stellar accretion rate via either approach increases the planetary accretion rate. For the $8\,M_\oplus$ model the inner planets (24 and 41 au) accrete $\sim 1\ M_\oplus$ each over the $\approx$ 15000 yrs of simulation time. Extrapolating this rate to over a million years leads to accretion of $\approx 50\ M_\oplus$, which is uncomfortably high. Increasing the disc viscosity also requires larger planets to form gaps initially as a greater gravitational torque is required to overcome the viscous torque from the gas (Dipierro et al. 2016).

The product of planetary mass and accretion rate $M_p\dot{M}_p$ for the outer planet (94 au) in the 0.3 M_J model is $2 \times 10^{-7}\ M_J^2/yr$, which is a factor of 5 greater than the upper limit deduced from Keck/NIRC2 vortex coronagraph observations (Ruane et al. 2017). Given that our model constrains the planet mass via the gap depth this suggests that the accretion rate may be too high in our model. We use a relatively large sink radius for computational reasons. A smaller sink radius may reduce the accretion rate, and improve agreement with the observed value.

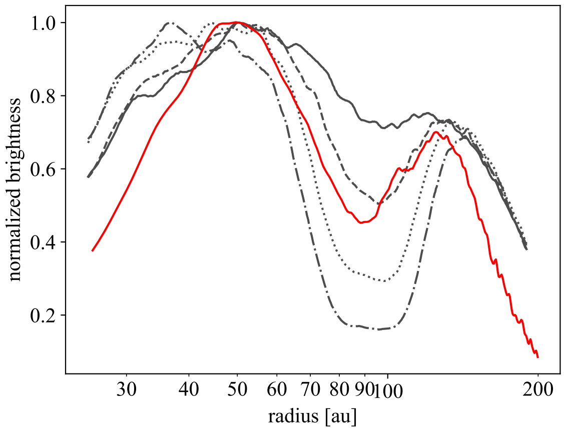

Figure 4. Azimuthally-averaged radial profile of 1.6 μm polarized intensity scaled by R^2. The solid, dashed, dotted, and dot-dashed lines are for 0.1, 0.3, 1, and 2 $\mathrm{M_J}$ gas-only models after 45 orbits. The red line is H-band SPHERE data from van Boekel et al. (2017). Each line is normalized to the bright ring peak at $\approx$ 40–50 au.

5 SUMMARY

We have performed global three-dimensional SPH simulations of a dusty disc with embedded protoplanets and produced synthetic observations of dust continuum, CO emission, and polarized scattered light to test our model against recent observations.

(i) We reproduce the gaps in dust emission in the ALMA observations of TW Hya with a 16–24 $\mathrm{M_\oplus}$ planet at 24 au and an 8–16 $\mathrm{M_\oplus}$ planet at 41 au, respectively.

(ii) We show that a giant planet (0.1–2.0 $\mathrm{M_J}$) at 94 au can explain the main gap in scattered light observations, and is consistent with CO observations. However, a spiral arm is also evident, for which there is only tentative evidence in the SPHERE image.

(iii) Our model requires a disc mass $\lesssim 10^{-3}\,\mathrm{M_\odot}$ in agreement with CO observations rather than the $> 0.05\,\mathrm{M_\odot}$ disc mass inferred by Bergin et al. (2013). A low mass disc is consistent with recent constraints on disc turbulence (Flaherty et al. 2018).

ACKNOWLEDGEMENTS

DM is funded by a Research Training Program Stipend from the Australian government. We acknowledge Australia Research Council funding via DP180104235, FT130100034, and FT170100040. We used gSTAR and OzStar, funded by Swinburne University of Technology and the Australian government, the MonARCH cluster at Monash, and SPLASH (Price 2007).

REFERENCES

Andrews S. M., et al., 2012, ApJ, 744, 162
Andrews S. M., et al., 2016, ApJ, 820, L40
Ayliffe B. A., Laibe G., Price D. J., Bate M. R., 2012, MNRAS, 423, 1450
Barrado Y Navascués D., 2006, A&A, 459, 511
Bate M. R., Bonnell I. A., Price N. M., 1995, MNRAS, 277, 362
Bergin E. A., et al., 2013, Nature, 493, 644
Béthune W., Lesur G., Ferreira J., 2016, A&A, 589, A87
Brickhouse N. S., Cranmer S. R., Dupree A. K., Günther H. M., Luna G. J. M., Wolk S. J., 2012, ApJ, 760, L21
Calvet N., D'Alessio P., Hartmann L., Wilner D., Walsh A., Sitko M., 2002, ApJ, 568, 1008
Debes J. H., Jang-Condell H., Weinberger A. J., Roberge A., Schneider G., 2013, ApJ, 771, 45
Debes J. H., et al., 2017, ApJ, 835, 205
Dipierro G., Price D., Laibe G., Hirsh K., Cerioli A., Lodato G., 2015, MNRAS, 453, L73
Dipierro G., Laibe G., Price D. J., Lodato G., 2016, MNRAS, 459, L1
Dong R., Fung J., 2017, ApJ, 835, 146
Duffell P. C., Dong R., 2015, ApJ, 802, 42
Epstein P. S., 1924, Physical Review, 23, 710
Flaherty K. M., Hughes A. M., Teague R., Simon J. B., Andrews S. M., Wilner D. J., 2018, ApJ, 856, 117
Flock M., Ruge J. P., Dzyurkevich N., Henning T., Klahr H., Wolf S., 2015, A&A, 574, A68
Gaia Collaboration et al., 2016, A&A, 595, A1
Gaia Collaboration Brown A. G. A., Vallenari A., Prusti T., de Bruijne J. H. J., Babusiaux C., Bailer-Jones C. A. L., 2018, preprint, (arXiv:1804.09365)
Gonzalez J.-F., Laibe G., Maddison S. T., 2017, MNRAS,
Haisch Jr. K. E., Lada E. A., Lada C. J., 2001, ApJ, 553, L153
Huang J., et al., 2018, ApJ, 852, 122
Hutchison M., Price D. J., Laibe G., 2018, MNRAS,
Johansen A., Youdin A., Klahr H., 2009, ApJ, 697, 1269
Kratter K., Lodato G., 2016, ARA&A, 54, 271
Laibe G., Price D. J., 2012, MNRAS, 420, 2345
Lodato G., Price D. J., 2010, MNRAS, 405, 1212
Nomura H., et al., 2016, ApJ, 819, L7
Pinte C., Ménard F., Duchêne G., Bastien P., 2006, A&A, 459, 797
Pinte C., Harries T. J., Min M., Watson A. M., Dullemond C. P., Woitke P., Ménard F., Durán-Rojas M. C., 2009, A&A, 498, 967
Poteet C. A., et al., 2018, preprint, (arXiv:1805.01926)
Price D. J., 2007, PASA, 24, 159
Price D. J., et al., 2017, preprint, (arXiv:1702.03930)
Ruane G., et al., 2017, AJ, 154, 73
Rycroft C. H., 2009, Chaos, 19, 041111
Shakura N. I., Sunyaev R. A., 1973, A&A, 24, 337
Simon J. B., Bai X.-N., Flaherty K. M., Hughes A. M., 2017, preprint, (arXiv:1711.04770)
Takeuchi T., Lin D. N. C., 2002, ApJ, 581, 1344
Thi W.-F., et al., 2010, A&A, 518, L125
Weidenschilling S. J., 1977, MNRAS, 180, 57
Zhang K., Blake G. A., Bergin E. A., 2015, ApJ, 806, L7
Zhu Z., Stone J. M., 2014, ApJ, 795, 53
van Boekel R., et al., 2017, ApJ, 837, 132
van't Hoff M. L. R., Walsh C., Kama M., Facchini S., van Dishoeck E. F., 2017, A&A, 599, A101